Applied Acoustics 73 (2012) 900–903

Contents lists available at SciVerse ScienceDirect

Applied Acoustics

journal homepage: www.elsevier.com/locate/apacoust

Nonlinear multi-frequency generation for underwater application

Lucilla Di Marcoberardino, Jacques Marchal *, Pierre Cervenka

UPMC Univ Paris 06, CNRS, UMR 7190, Institut Jean le Rond d'Alembert, 2 Place de la Gare de Ceinture, 78210 Saint-Cyr-l'Ecole, France

ARTICLE INFO

Article history:
Received 19 May 2011
Accepted 20 March 2012
Available online 18 April 2012

Keywords:
Multi-frequency transmitter
Seafloor characterization
Nonlinear propagation

ABSTRACT

This study examines the feasibility of designing a multi-frequency acoustic surveying tool based on the saturation effect. The transmitter is driven by a high-power single tone-burst: nonlinear propagation creates the beams at harmonic frequencies. A simple pseudo one-dimensional model is used to estimate the expected on-axis harmonic levels generated with a rectangular aperture. First measurements are reported and compared with the estimations.

© 2012 Elsevier Ltd. All rights reserved.

1. Introduction

Classical acoustical surveying systems collect seafloor data usually on a narrow frequency bandwidth; a single system does not provide frequency diversity in the collected acoustic backscattered echoes. The ability to collect data at different frequencies would be an interesting asset for seafloor characterization. Geological surveys, industrial monitoring of underwater structures, and environmental protection are potential applications [1]. For example, the interest in the multi-frequency approach has been put in evidence in a study on the capability to detect sunken oil slicks [2]. Results showed that high-frequency sources revealed the presence of flat superficial spots (specular reflection, no backscattered energy), whereas low-frequency responses showed the underlying substrate (transmission through the thin layer of oil). The combination of all acquired information makes it possible to deduce the presence of oil slicks. At the present time, gathering multi-frequency information implies the use of different systems [3]. Consequently, the collected data are not perfectly matched in time and space, and their fusion is problematic.

This study investigates the feasibility of an original system that takes advantage of nonlinear propagation to achieve a multifrequency source. The principle is to generate a harmonic pulse with sufficient energy so that the saturation phenomenon emerges [4–6]. As a result, a single source generates a whole set of beams at harmonic frequencies, and all these beams are perfectly superposed both in time and in space. From a practical point of view, it is desirable that the beam patterns feature a large aperture along one dimension. Hence, the difficulty lies in designing a transmitter that produces harmonic beams with such a geometry, while keeping sufficient source levels. We present here the advances and trials results with a rectangular array. Preliminary orders of magnitude have been set with a simple pseudo one-dimensional (1D) model. Experimental results are presented, and are compared with the numerical estimations.

2. Pseudo 1D model

2.1. Theory

It is a common practice to model finite-amplitude fields of progressive acoustic waves with the Khokhlov-Zabolotskaya-Kuznetsov (KZK) equation [7]. The model is based on the assumption that the sound beam is confined around the paraxial region. A few attempts to model the acoustical fields generated with wider apertures can be found in the literature [8]. To evaluate the on-axis multi-frequency levels that can be expected using elongated rectangular sources, we use a simple pseudo-1D model. It is based on the generalized Burgers equation [9], taking into account attenuation, diffraction, and nonlinear phenomena. We recall here some highlights of this model.

The wave energy is assumed to be collimated in the near field (plane wave propagation) and uniformly distributed over a cone in the far field (spherical spreading). For a rectangular projector, a transition region featuring cylindrical propagation has to be considered in between (see Fig. 1).

The transitions between these three regions occur respectively at the Fraunhofer (or Rayleigh) distances $L_{FA} = A^2/\lambda_0$ and $L_{FB} = B^2/\lambda_0$, where A and B denote the characteristic dimensions of the source and λ_0 is the wavelength at the fundamental frequency f_0. The angles delimiting the beamwidth in the cylindrical and spherical regions correspond to the half-apertures at -3 dB, θ_A and θ_B. The main hypothesis in this model is that the acoustic field

* Corresponding author.
E-mail address: jacques.marchal@upmc.fr (J. Marchal).

0003-682X/$ - see front matter © 2012 Elsevier Ltd. All rights reserved.
http://dx.doi.org/10.1016/j.apacoust.2012.03.011

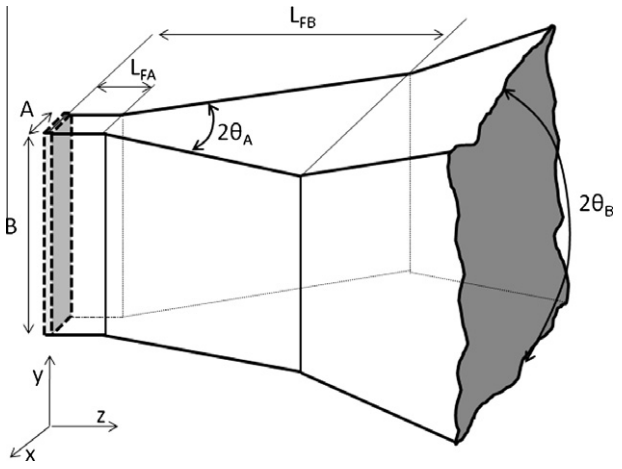

Fig. 1. Scheme of the energy distribution [10].

is homogeneous within each defined zone. Expressing the Laplacian operator in terms of radial coordinate r, the pressure depends only on $r = |r|$ and t. Because it is a pseudo-1D model, one imposes $r = z$ in the plane wave zone. The model can be expressed in terms of pressure by the equation:

$$\frac{\partial P}{\partial r} = -\mathcal{L}(P) - \frac{m}{r}P + \frac{\beta}{2\rho_0 c_0^3}\frac{\partial (P)^2}{\partial t} \text{ with } m = \begin{cases} 0 & \text{if } r < L_{FA} \\ 1/2 & \text{if } L_{FA} \leqslant r < L_{FB} \\ 1 & \text{if } r \geqslant L_{FB} \end{cases} \quad (1)$$

where c_0 is the sound speed and β is the coefficient of nonlinearity ($\beta = 3.5$ in fresh water). The coefficient m takes into account the diverging propagation loss: $m = 0$, 1/2, 1, respectively for plane, cylindrical and spherical waves. Actually, Eq. (1) is the combination of the generalized Burgers equation for diverging waves (see Eq. (58) in Chapter 3, Ref. [7]) propagating in dispersive media [9]. $\mathcal{L}(P)$ is a linear operator that describes different phenomena related to attenuation as thermoviscous attenuation and dispersion due to relaxation process. From a practical point of view, attenuation can be considered a function of frequency f by using the attenuation coefficient $\alpha(f)$:

$$\mathcal{L}(e^{j2\pi ft}) = \alpha(f)e^{j2\pi ft} \quad (2)$$

In sea water, the Francois-Garrison model [11] is commonly admitted.

Denoting v_0 as the velocity normal to the projector surface, Eq. (1) can be written in the dimensionless form with $p = P/\rho_0 c_0 v_0$:

$$\frac{\partial p}{\partial r} = -\frac{m}{r}p - \frac{1}{L_\alpha}\mathcal{L}'(p) + \frac{1}{L_S}p\frac{\partial p}{\partial \tau} \quad (3)$$

Eq. (3) outlines the influence of all the phenomena that dictate the pseudo-1D propagation through the following characteristic distances: $L_\alpha = 1/\alpha(f_0)$ is the attenuation distance, $L_S = {c_0}^2/2\pi\beta v_0 f_0$ is the shock formation distance, $\tau = 2\pi f_0 t$ is the dimensionless time, and $\mathcal{L}' = \mathcal{L}/\alpha(f_0)$ is the dimensionless attenuation propagator that simplifies into $\mathcal{L}' = \partial^2/\partial\tau^2$ for pure fresh water. The relative magnitudes of the lengths L_S, L_F, and L_α reveal the relative influence of each effect during the propagation. The nonlinear phenomenon is observable if L_S is shorter than the other two distances, i.e. the Khokhlov number $K = L_F/L_S$ and the Gol'dberg number $\Gamma = L_\alpha/L_S$ are larger than unity.

2.2. Numerical implementation

The numerical code is developed by using the fractional-step procedure performed along the main propagation direction r [12]. The main phenomena occurring during propagation are processed consecutively at each step Δr. The second-order accuracy can be reached by using, for instance, the Strang splitting scheme [13]. Hence, the step value is derived from a reference length that is defined as the smallest of L_α, L_F, and L_S. Another point to be considered is the choice of the computational domain in the numerical implementation. The results presented next are obtained with a hybrid method [14]: geometrical spreading and absorption are solved in the frequency domain while nonlinearity is solved in the time domain. The first two contributions are handled with the exact solutions, i.e.

$$\frac{\partial p}{\partial r} + \frac{m}{r}p = 0 \;\rightarrow\; p/r^m = \text{const} \quad (4)$$

$$\frac{\partial p}{\partial r} = -\frac{1}{L_\alpha}\mathcal{L}'(p) \;\rightarrow\; p(f)e^{+\alpha(f)r} = \text{const} \quad (5)$$

The nonlinear contribution is evaluated by using a development of the implicit Poisson solution:

$$\frac{\partial p}{\partial r} = \frac{1}{L_s}p\frac{\partial p}{\partial \tau} \;\rightarrow\; p(r+\Delta r,\tau) \approx p\left(r, \tau + p\frac{\Delta r}{L_s}\right) \quad (6)$$

The solution is obtained in this scheme by interpolating the sound pressure signal at each step with a distorted time. To avoid multi-valued solutions, it is sufficient to take provision that the maximum time shift in Eq. (6) remains smaller than the numerical time sampling $\Delta\tau$ – i.e. $\max(|p|)\Delta r/L_S \leqslant \Delta\tau$. This condition is always verified if $\Delta r \leqslant L_S/N$, where N denotes the number of samples per period.

Detailed descriptions of the pseudo-1D model and its numerical implementation can be found in [15].

3. Experimental set-up

A rectangular source is designed to transmit a $1^\circ \times 25^\circ$ aperture beam at 100 kHz. The size of the array is 3.1 cm × 78 cm. With a 1.5 cm wavelength, the corresponding Fraunhofer distances are 6 cm and 40 m. The transmitting voltage response is 176 dB re 1 μPa/V@1 m.

3.1. Set-up

The source is tested in the sea water tank (50 m × 12.5 m × 10 m) at the Ifremer facilities in Brest (France). The array is deployed from a mobile deck that enables rotational and translational movements. The receiving chain consists of a hydrophone (Reson TC4034) connected to the acquisition system NI PXIE 6366 via a preamplifier (Reson VP1000). Because of the hydrophone bandwidth (1 Hz–500 kHz), only the measurements on the first five harmonics are reported. During the experiments, the sound speed is 1507 m/s (derived from the Lovett model [16] with $T = 14.9$ °C and salinity of 35.5‰). The attenuation distance is $L_\alpha = 235$ m at the fundamental frequency (denoted F0 or H1).

Table 1
Source levels (dB re 1 μPa rms) and shock distance versus input power.

P_e	P_0	P at 1 m	L_S
1.2 kW	221 dB	225 dB	6.9 m
5 kW	227 dB	231 dB	3.6 m
20 kW	233 dB	237 dB	1.8 m

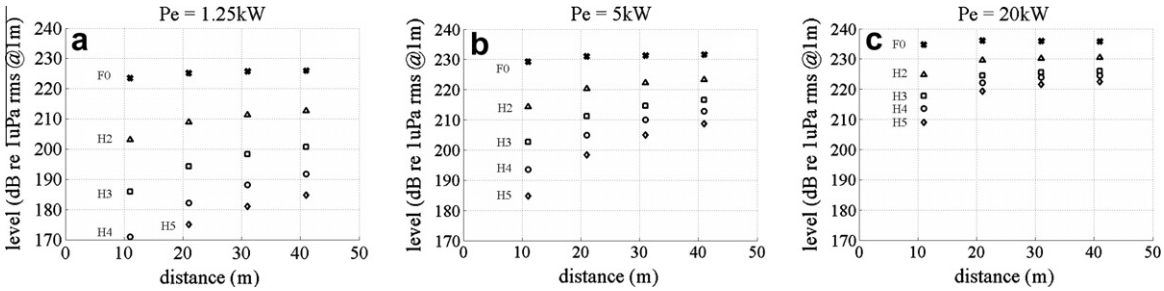

Fig. 2. Harmonics' level versus distance for three applied electrical powers P_e. (a) P_e = 1.25 kW, (b) P_e = 5 kW and (c) P_e = 20 kW.

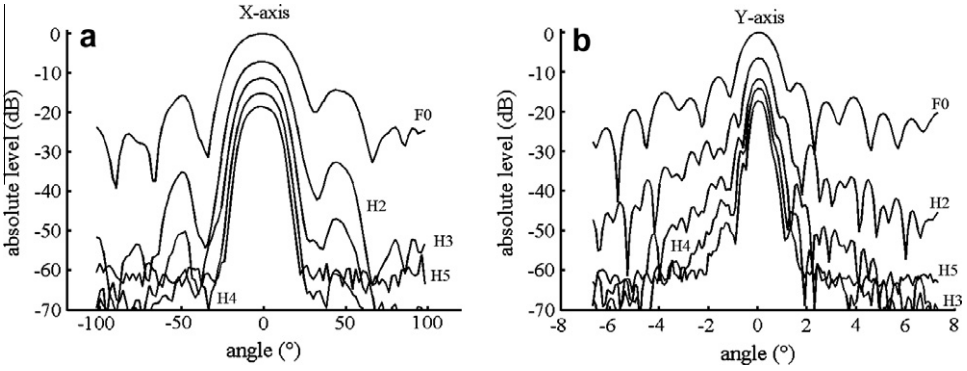

Fig. 3. Directivity of the first five harmonics (z = 41.4 m, P_e = 20 kW) (a) x-axis and (b) y-axis.

Note that the attenuation distance for higher harmonics ranges between 133 m (second harmonic H2) and 54 m (fifth harmonic H5). The power is provided by a custom E/D class amplifier that delivers up to 20 kW electric power. Because the output signal is square shaped, its spectral content is a combination of odd harmonics. Past experiences have shown that the components of these frequencies interfere destructively with the harmonics generated by nonlinear propagation. Consequently, a filter is inserted in the matching circuit. The rejection of all the harmonics is better than −30 dB. The source level at the fundamental frequency can be directly estimated from the voltage driving the array and the sensitivity of the transducer (established at low transmitting levels). Table 1 shows the acoustic levels obtained as a function of the nominal electric power delivered by the amplifier (the global electro-acoustic efficiency of the transmitter is in the range of 65–70%). When the characteristic distances are compared, it appears that L_α is always much larger than L_S and L_F, so that the attenuation is never the dominant effect. On the other hand, it can be seen that diffraction and nonlinearity are competing effects: L_S is included in the cylindrical zone.

Working in piston mode, the active surface of the transmitters is driven with a uniform normal velocity v_0. In Table 1, the equivalent pressure is defined as $P_0 = \rho_0 c_0 v_0$. The cavitation threshold depends on different parameters, such as frequency, pulse length, and static pressure. A significant clue that no cavitation occurs is that repeated measurements exhibit very stable results.

4. Results

4.1. On-axis levels

Fig. 2 shows the on-axis levels measured for the first five harmonics. They are presented as source levels, i.e. compensated for a pseudo spherical divergence, and linear attenuation. However, being the result of a nonlinear generation along the propagation, these values are relevant at the distance of observation. The array is driven with three different electrical powers. At the lower end (1.25 kW), there is a weak nonlinear production. For example, the H5 harmonic is 50 dB below the level of the fundamental F0, hence close to the noise threshold. On the other hand, at maximum electrical power, all the equivalent source levels are in the range of 219 dB to 236 dB re 1 μPa rms@1 m beyond a 20 m range. The elongated rectangular geometry was thought to be very penalizing because of the large aperture along one principal side. Nevertheless, it can be seen that very close, and still large source levels can be achieved for the first harmonics.

Table 2
3 dB beam-width measured at 41 m from the array.

	P_e = 1.25 kW		P_e = 5 kW		P_e = 20 kW	
	x-axis	y-axis	x-axis	y-axis	x-axis	y-axis
H1	24°	1.04°	25°	1.06°	29°	1.15°
H2	17°	0.62°	18°	0.65°	24°	0.78°
H3	14°	0.52°	15°	0.52°	21°	0.66°
H4	12°	0.51°	13°	0.51°	20°	0.59°
H5	–	–	12°	0.51°	19°	0.54°

4.2. Beam pattern

Fig. 3 shows the directivity patterns measured at a 41 m distance, using the maximal power. Table 2 reports the characteristic −3 dB apertures obtained with the different applied powers. Measurements are performed in a plane perpendicular to the z-axis, i.e. not at a constant range. It can be observed that the higher the harmonic, the narrower the aperture. However, the beam-width does not depend linearly on frequency. Note that the fifth harmonic is affected by noise. The beamwidth of each harmonic becomes larger with the increase of the transmission level (Table 2).

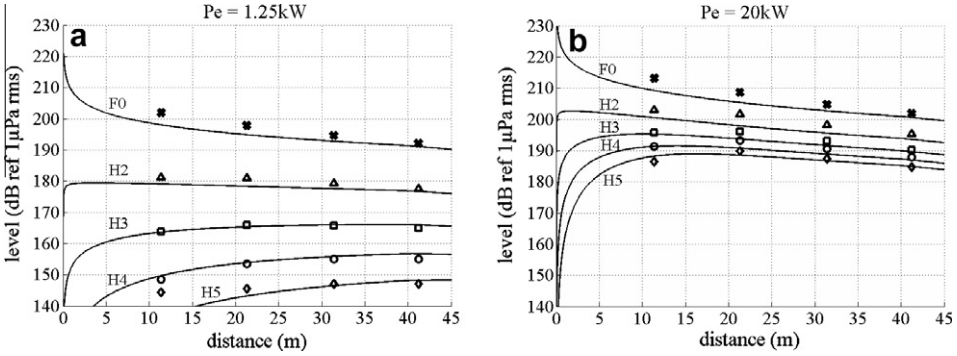

Fig. 4. Acoustic level of the five harmonics versus range. Simulation and experimental results (a) P_e = 1.25 kW and (b) P_e = 20 kW.

4.3. Comparison with numerical estimations

The on-axis levels measured at different distances are compared with the estimations obtained with the pseudo-1D model in Eq. (3). Fig. 4 shows a good agreement between simulations and measurements. However, the model tends to underestimate the experimental data. Note that the discrepancy observed with H5, at close range from the transmitter and low electrical power, is mostly caused by the poor signal-to-noise ratio of the experimental records.

5. Conclusions

A multi-frequency source that takes advantage of the saturation effect is studied. The beam aperture ($1^\circ \times 25^\circ$) is sizeable with a sidescan sonar application. Although the aperture is relatively broad in one plane (25°), the equivalent source levels measured with the first generated harmonics show satisfactory values. A model has been used to estimate the on-axis levels produced by a rectangular aperture. Although very simple, it shows a reasonable agreement with the experimental data. Hence, this model qualifies for a first-design dimensioning. The next step of this study will be to test the source in the sea environment to record backscattered echoes from several seafloor sediments. In addition, a more accurate three-dimensional model must be built.

Acknowledgments

This project has been funded by IFREMER. The authors are grateful for the assistance provided by Yves Le Gall during the experimental measurements.

References

[1] Blondel P. The handbook of sidescan sonar. Springer-Praxis; 2009.
[2] Parthiot F, de Nanteuil E, Merlin F, Zerr B, Guedes Y, Lurton X, Augustin J-M, Cervenka P, Marchal J, Sessarego J-P, Hansen RK. Sonar detection and monitoring of sunken heavy fuel oil on the seafloor. NOSCA. In: Proceedings interspill conference, trondheim. 2004. 14–17 June. <http://www.interspill.com/previous-events/2004/pdf/session6/465_PARTHIOT.pdf>.
[3] Lurton X, Legac J-C. The CALIMERO project: scientific objectives and first at-sea results. In: Proc. SeaTechWeek, In situ seabed characterization. Brest; 2004 [21–22 October].
[4] Muir TG. Nonlinear effects in acoustic imaging. Acoust Imag 1980;9:93–109.
[5] Shooter JA, Muir TG, Blackstock DT. Acoustics saturation of spherical waves in water. J Acoust Soc Am 1974;55:54–62.
[6] Novikov BK, Rudenko OV, Timoshenko VI. Nonlinear underwater acoustics. Translation series. New York: American Institute of Physics; 1987.
[7] Hamilton MF, Blackstock DT. Nonlinear acoustics. Texas: Academic Press; 2002.
[8] Rénier M, Dragau F, Marchiano R, Coulouvrat F. HOWARD: un modèle pour la propagation d'ondes de choc acoustiques en milieu hétérogène, au-delà de l'approximation parabolique. Lyon: 10ème Congrès Français d'Acoustique; 2010 [12–16 April].
[9] Blackstock DT. Generalized Burgers equation for plane waves. J Acoust Soc Am 1985;77:2050–3.
[10] Moffett MB, Mellen RH, Konrad WL. Parametric acoustic sources of rectangular aperture. J Acoust Soc Am 1978;63:1326–31.
[11] Francois RE, Garrison GR. Sound absorption based on ocean measurements. Part II: boric acid contribution and equation for total absorption. J Acoust Soc Am 1982;72:1879–90.
[12] Ames WF. Numerical methods for partial differential equations. Boston: Academic Press; 1992.
[13] Strang G. On the construction and comparison of difference schemes. SIAM J Numer Anal 1968;5:506–17.
[14] Bakhvalov NS. Nonlinear theory of sound beams. New York: American Institute of Physics; 1987.
[15] Di Marcoberardino L, Marchal J, Cervenka P. Nonlinear multi-frequency transmitter for seafloor characterization. Acta Acustica/Acustica 2011;97:202–8.
[16] Lovett JR. Merged seawater sound-speed equations. J Acoust Soc Am 1978;63:1713–8.